



Conference Proceedings Paper – Remote Sensing

Using Simplified Thermal Inertia to Determine the Theoretical Dry Line in Feature Space for Evapotranspiration Retrieval

Sujuan Mi^{1,2}, Hongbo Su^{3,*}, Renhua Zhang¹, Jing Tian¹

¹ Key Laboratory of Water Cycle & Related Land Surface Processes, Institute of Geographic Sciences and Natural Resources Research, Beijing 100101, China

² University of Chinese Academy of Sciences, Beijing 100049, China

³ Department of Civil, Environmental and Geomatics Engineering, Florida Atlantic University, Florida, USA 33431; E-mail: hongbo@ieee.org

* Author to whom correspondence should be addressed; E-mail: hongbo@ieee.org;
Tel.: +1-561-297-3936.

Published: 23 June 2015

Abstract: With the development of quantitative remote sensing, regional evapotranspiration (ET) modeling based on the feature space has made substantial progresses. Among those feature space based evapotranspiration models, accurate determination of the theoretical dry/wet lines remains a challenging task. This paper reports the development of a new method, named DDTI (Determination of Dry line by Thermal Inertia), which determines the theoretical dry line based on the relationship between the thermal inertia and the soil moisture. The Simplified Thermal Inertia value estimated in the North China Plain is consistent with the value measured in the laboratory. Two evaluation methods, which are based on the comparison of the locations of the theoretical dry line determined by two models (DDTI and the heat energy balance method) and the comparison of the Evaporative Fraction between the estimates from the two models and the in situ measurements, were used to assess the performance of the new method DDTI. The location of the theoretical dry line determined by DDTI is more accurate than that determined by the heat energy balance method. When compared with the in situ measurement of Evaporative Fraction (EF) at Yucheng Experimental Station, the ET model based on DDTI reproduces the pixel scale EF with an RMSE (Root Mean Square Error) of 0.095, which is much lower than that based on the heat energy balance method with an RMSE of 0.224. Also, the bias between the DDTI method and the in situ measurements is 0.069, lower than the bias of the heat energy balance method, which is 0.168.

Keywords: Thermal inertia; two-layer evapotranspiration model; theoretical dry line; evapotranspiration; remote sensing

1. Introduction

Evapotranspiration (ET) monitoring has important implications in many aspects, such as improving regional and global climate models, understanding the hydrological cycle, and assessing environmental stress on natural and agricultural ecosystems [1, 2]. With the development of Remote Sensing technology, estimating regional ET has made great progresses [3, 4, 5, 6]. Satellite-based ET modeling can be categorized into one-layer schemes and two-layer schemes. Examples of the one-layer scheme include the Surface Energy Balance Algorithm (SEBAL) [7], the Surface Energy Balance (SEBS) [8], and the Simplified Surface Energy Balance Index (S-SEBI) [9]. Some representative two-layer models are N95 [10], the two-source energy balance approach [11], and the operational two-layer Remote Sensing model [12]. In the one-layer model, a mixed pixel composed of vegetation and soil is treated as a block. These one-layer models are suitable for regions with homogeneous dense vegetation or bare soil, but in many regions, such as semi-arid regions where patches of vegetation and bare soil are mixed, two-layer models perform much better than one-layer models. Two-layer models can estimate evaporation from soil and transpiration from vegetation separately, which is an important progress in the ET modeling. In the two-layer model, separating vegetation temperature and soil temperature is the most important procedure. One method to separate temperatures is to use the Priestly-Taylor factor, proposed by Norman [10]. This method estimates evapotranspiration and the vegetation temperature by using the Priestly-Taylor factor first; then, the soil temperature can be estimated from the land surface temperature, vegetation cover fraction, and vegetation temperature. However, determining an optimal value for the Priestly-Taylor factor is difficult in this method. Norman first chose a value of 1.3, then Kustas and Norman changed the Priestly-Taylor factor to 2 [13]. Later, Komastu reported that 1.26 was more reasonable in wet areas and that it should be smaller in dry areas [14]. Another method to separate temperature, named PCACA (Pixel Component Arranging and Comparing Algorithm), was proposed by Zhang and separates temperatures based on the hypothesis of a linear mixing structure of vegetation and soil in a pixel [12].

The third method to retrieve evapotranspiration is based directly on the relationship between the vegetation index and the land surface temperature and is known as the feature space method [4, 15, 16, 17]. The advantage of using the feature space method is that complex parameterization of aerodynamic and surface resistances for water and heat transfer can be avoided; meanwhile, the feature space of VFC_LST (vegetation fraction cover *versus* land surface temperature) is able to capture the availability of soil moisture essential for evapotranspiration. The feature space method has been used widely by the remote sensing community. As Carlson has noted, when a large number of pixels exist in the study area and exceptional pixels are removed, a triangular shape exists in the feature space [18]. In order to apply the CWSI (Crop Water Stress Index) to partially-vegetated fields, Moran proposed a Vegetation Index/ Temperature (VIT) trapezoid model [16].

The location of the theoretical dry/wet line within the feature space directly affects the performance of the space feature method. The theoretical dry line corresponds to the pixels with the largest water stress and zero ET. The theoretical wet line corresponds to the pixels without any water stress and ET is close to the potential evapotranspiration. In previous studies, the theoretical wet line was usually determined by the lowest land surface temperature in the image or by the temperature of nearby bodies of water. The theoretical dry line, though, is more difficult to determine due to the existence of abnormal or false dry pixels. Tang presented an iterative algorithm to automatically determine the theoretical dry line [17]. The algorithm firstly segments the whole fractional vegetation cover region into M bins; secondly, the abnormal pixels are removed according to the mean value and standard deviation of each bin; thirdly, the highest values in each bin are chosen as values to determine the theoretical dry line; finally, the dry line is determined by a linear regression of the highest values. Tang's method can determine the theoretical dry line quickly, but for wet areas, such as after a rainfall, the dry line obtained is not the "true" theoretical dry line because dry pixels are not available.

An evapotranspiration method named the two-layer Remote Sensing model was proposed first by Zhang [12] and was then optimized by Zhang in 2008 [18]. In this method, the positions of the theoretical dry line and the theoretical wet line (especially the dry line) are key parameters. Zhang's method is based on the heat energy balance method, and air temperatures are used to calculate the sensible heat flux. Air temperature data are obtained from nearby weather stations. This method can determine the theoretical dry line, but in wet weather, the dry line determined is not the true theoretical dry line because air temperatures are obtained from wet cases. The method based on the heat energy balance equation is called the heat energy balance model in this article. This method will be discussed in detail in section 2.

Since there is insufficient study on the determination of the theoretical dry line's location, this paper proposes a new method based on thermal inertia to obtain the theoretical dry line in the feature space, and it will be compared with the heat energy balance method using the same data set in order to provide an insight into the performance of two models. Section 2 presents the methodology of both the new method (DDTI) and the heat energy balance method. Experimentation results and a laboratory evaluation of the thermal inertia are shown in Section 3, followed by an application of the DDTI method in Section 4. Finally, conclusions are given in Section 5.

2. Methodology

2.1 The heat energy balance method

In the two-layer remote sensing model [18], there are three main procedures in the ET estimation: the first is the PCACA method to decompose the temperature of the mixed pixels; the second is to determine the location of the theoretical dry and wet lines by heat energy balance equations; the third is the layered energy-separating algorithm to determine the Bowen Ratio. The detailed description of the three procedures can be found in Zhang (2008) [18]. We focus on how to determine the theoretical dry line in this paper. For pixels on the theoretical dry line, ET is equal to 0. Based on the heat energy balance equation, Eq. (1) can be derived

$$R_n - G = H \quad (1)$$

where R_n is the net radiation, G is soil heat flux, and H is the sensible heat flux.

According to the empirical correlation between soil heat flux and the net radiation, G can be estimated by Eq. (2) [18].

$$G = 0.3 * (1 - 0.9f)R_n \quad (2)$$

where f is the vegetation fraction cover.

The sensible heat flux and the net radiation can be estimated by Eq. (3) and Eq. (4), respectively.

$$H = \frac{\rho C_p (T_{sd} - T_{sda})}{r_{sda}} \quad (3)$$

$$R_n = S_0(1 - \alpha_{sd}) + \sigma \varepsilon_{sky} T_{sky}^4 - \sigma \varepsilon_{sd} T_{sd}^4 \quad (4)$$

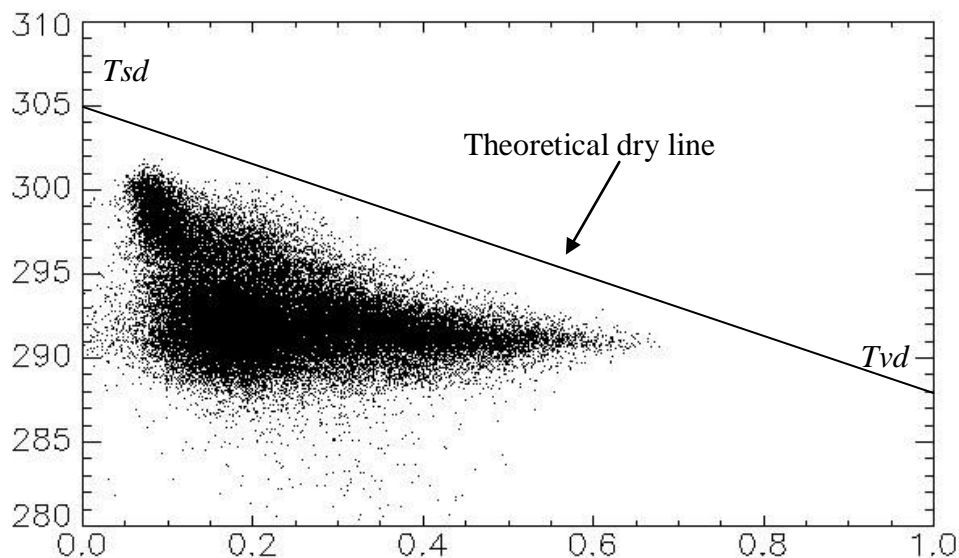
The temperature of the theoretical dry bare soil surface in Eq. (5) can be deduced by Equations 1 to 4.

$$T_{sd} = \frac{0.7[S_0(1 - \alpha_{sd}) + \sigma \varepsilon_{sky} T_{sky}^4] + \frac{\rho C_p}{r_{sda}} T_{sda}}{\frac{\rho C_p}{r_{sda}} + 0.7\sigma \varepsilon_{sd} T_{sd}^3} \quad (5)$$

$$T_{vd} = \frac{0.7[S_0(1 - \alpha_{vd}) + \sigma \varepsilon_{sky} T_{sky}^4] + \frac{\rho C_p}{r_{vda}} T_{vda}}{\frac{\rho C_p}{r_{vda}} + 0.7\sigma \varepsilon_{vd} T_{vd}^3} \quad (6)$$

In the same way, the temperature of a theoretical dry surface with a full vegetation cover can be described by Eq. (6). In the above equations, T_{sd} and T_{vd} are the surface temperatures of the two endpoints on the theoretical dry line (Figure 1), ρ is density of air, C_p is the volumetric heat capacity of air, r_{sda} and r_{vda} are the air dynamic resistance, ε_{sd} and ε_{vd} are the emissivity of bare soil area and full vegetation coverage, σ is the Stefan-Boltzmann Constant, S_0 is the solar incident total radiation, α_{sd} and α_{vd} are the albedo of dry bare soil and full vegetation coverage, ε_{sky} is the emissivity of the sky, and T_{sda} and T_{vda} are the air temperatures above the bare soil area and the full cover vegetation area, respectively.

Figure 1. Schematic figure of the theoretical dry line in the feature space of Temperature (in K) and VFC



According to Eq. (1) and Eq. (3), the difference between T_{sd} and T_{sda} can be expressed by Eq. (7). Then, the land surface temperature can be calculated by Eq. (8).

$$T_{sd} - T_{sda} = \frac{(R_n - G)r_{sda}}{\rho C_p} \quad (7)$$

$$T_{sd} = T_{sda} + \frac{(R_n - G)r_{sda}}{\rho c_p} \quad (8)$$

It can be seen from Eq. (8) that the air temperature is closely related to the land surface temperature. In the heat energy balance method, the heat energy balance is reinforced in each step. The variable controlling the sensible heat is actually the difference between air temperature and land surface temperature, not the air temperature alone. With a fixed sensible heat value and a fixed air dynamic resistance, the difference between air temperature and land surface temperature is also a constant. However, there are numerous solutions for the pairs of temperatures that can meet the above requirement of a constant temperature difference. As is known, because of the active land-atmosphere interactions, the air temperature in wet weather has a larger deviation from that of dry weather. Therefore, it is not reasonable to apply the air temperatures observed in wet conditions to determine the location of the theoretical dry line.

2.2 The thermal inertia method

Thermal inertia represents the resistance to change in the temperature of the upper few centimeters of the surface throughout the day, and it is independent of the local time, latitude, and the season [19]. Thermal inertia is defined as

$$P = \sqrt{K \rho_s c} \quad (9)$$

where P is the thermal inertia in $\text{Jm}^{-2}\text{K}^{-1}\text{s}^{-1/2}$ or $\text{cal} \cdot \text{cm}^{-2} \cdot \text{s}^{-1/2} \cdot \text{°C}^{-1}$, K is the thermal conductivity in $\text{Jm}^{-2}\text{K}^{-1}\text{s}^{-1/2}$, ρ_s is the density in gm^{-3} , and c is the specific heat capacity in $\text{Jm}^{-2}\text{K}^{-1}$. For wet soil, based on the linear mixture model, its thermal inertia can be described by Eq. (10) [20].

$$P_{ws} = \frac{V_s P_s + V_w P_w}{V_s + V_w} \quad (10)$$

where P_{ws} , P_s , and P_w are thermal inertia for wet soil, dry soil, and water, respectively. V_s and V_w are the volumetric proportions of soil and water in a soil sample. The dry soil has a minimal water content, and its thermal inertia depends on soil type and structure. Thermal inertia for dry soil will remain the same if its type and structure do not change. In this paper, we use a method named Simplified Thermal Inertia (STI), defined in Eq. (11). Thermal inertia can be estimated by soil heat flux. However, this method cannot be used in dense vegetation-covered areas because soil heat flux cannot be directly estimated by remote sensing in full cover vegetation areas. The net radiation can be estimated by remote sensing methods with high accuracy; therefore, the net radiation is used to calculate the thermal inertia. The thermal inertia result by the net radiation is different from that by the soil heat flux, so this method is called simplified thermal inertia (STI).

$$P_s = \frac{R_{ns} \sqrt{(t_2 - t_1)}}{T_{s2} - T_{s1}} \quad (11)$$

where P_s is the STI for soil, t_1 and t_2 are the start and end times of the measurements, T_{s1} and T_{s2} are the soil surface temperatures at t_1 and t_2 , and R_{ns} is the mean net radiation from t_1 to t_2 .

According to the above definition, the simplified thermal inertia for dry soil can be estimated from an extremely dry situation in a historical period. For example, the thermal inertia value P_{sd} of a historical dry situation can be calculated by Eq. (12). Then, P_{sd} can be used in a wet situation in Eq. (13) in order to derive the temperatures on the theoretical dry line. T_{s2h} is the theoretical dry temperature.

$$P_{sd} = \frac{R_{nsd} \sqrt{t_{2d} - t_{1d}}}{T_{s2d} - T_{s1d}} \quad (12)$$

$$T_{s2h} = \frac{R_{nsh}\sqrt{t_{2h}-t_{1h}}}{P_{sd}} + T_{s1h} \quad (13)$$

where t_{1d} and t_{2d} are the start and end times of the measurements in a dry situation. T_{s1d} and T_{s2d} are the soil surface temperatures at t_{1d} and t_{2d} , R_{nsd} is the mean net radiation from time t_{1d} to time t_{2d} , t_{1h} and t_{2h} are the start and end times of measurements in a wet situation, T_{s1h} and T_{s2h} are the soil surface temperatures at t_{1h} and t_{2h} , and R_{nsh} is the mean net radiation from time t_{1h} to t_{2h} .

In Eq. (13), all of the variables on the right hand side except P_{sd} are observed in a wet situation. In this paper, the method for calculating the simplified thermal inertia P_{sd} from a dry situation that is then used in a wet situation is called DDTI (Determination of Dry line by Thermal Inertia)

As is known, soil thermal inertia cannot be estimated by remote sensing in vegetation covered areas [21]. Although the mechanism of determining surface temperature change of vegetation is quite different from the mechanism of determining the surface temperature change of soil, the diurnal cycle of vegetation surface temperature is quite similar to that of soil. Moreover, the daily amplitude for vegetation surface temperature, which is proportional to radiation input and inversely proportional to water availability, is also similar to surface temperature of soil. The formula of STI for vegetation is shown in Eq. (14).

$$P_v = \frac{R_{nv}\sqrt{(t_2-t_1)}}{T_{v2}-T_{v1}} \quad (14)$$

where P_v is the STI for vegetation, t_1 and t_2 are the start and end times of measurements, T_{v1} and T_{v2} are surface temperatures at time t_1 and t_2 , and \bar{R}_{nv} is the mean net radiance from time t_1 to t_2 .

For wet areas with a full vegetation cover, we use a method similar to that used for bare soil areas in order to calculate the surface temperature of the theoretical dry point. That is to say, we first calculate P_{vd} in a dry situation, and then apply it to a wet situation. Formulas are given in Eq. (15, 16).

$$P_{vd} = \frac{R_{nvd}\sqrt{t_{2d}-t_{1d}}}{T_{v2d}-T_{v1d}} \quad (15)$$

$$T_{v2h} = \frac{R_{nvh}\sqrt{t_{2h}-t_{1h}}}{P_{vd}} + T_{v1h} \quad (16)$$

where t_{1d} and t_{2d} are the start and end times of measurements in dry situations. T_{v1d} and T_{v2d} are soil surface temperatures at t_{1d} and t_{2d} , R_{nvd} is the mean net radiation from time t_{1d} to t_{2d} , t_{1h} and t_{2h} are the start and end times of measurements in wet situations, T_{v1h} and T_{v2h} are soil surface temperatures at time t_{1h} and t_{2h} , and R_{nvh} is the mean net radiation from time t_{1h} to t_{2h} .

3. Experiment and laboratory evaluation of the thermal inertia model

3.1 Computing simplified thermal inertia

3.1.1. Selecting clear days in the study area.

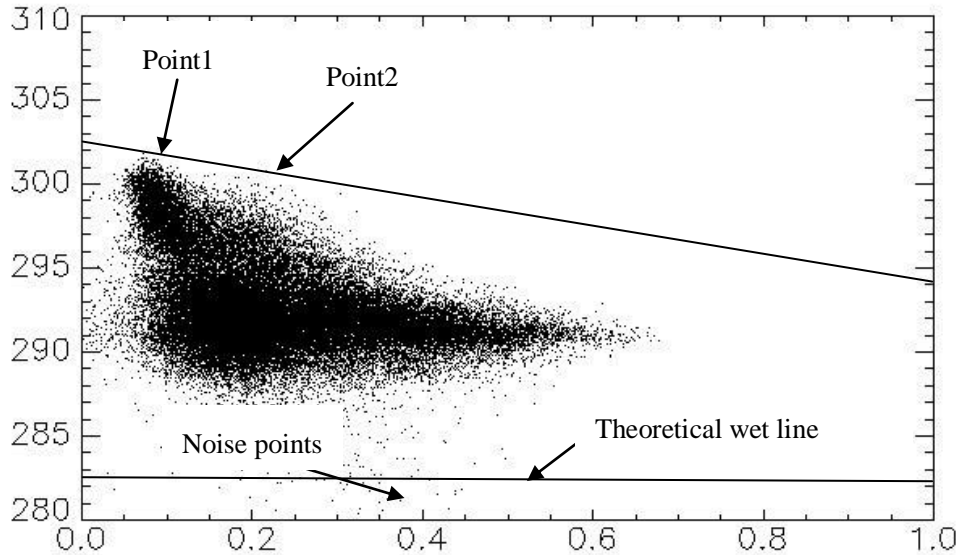
Based on historical data from the China Meteorological Data Sharing Service System, it was found that in the spring of 2011, the North China Plain experienced an extremely dry period: the accumulative precipitation of spring 2011 (8mm) was much less than the average spring accumulative precipitation of the previous thirty years (22.5mm). So, spring of 2011 is an ideal period to calculate the simplified thermal inertia for dry soil. The MOD11A1 data were used to choose clear sky days, and

from March 1 to April 30 in 2011, 7 days met the requirements (cloud cover less than 10%). The 7 days are March 10, March 17, March 30, April 4, April 11, April 18, and April 24.

3.1.2. Computing STI

a) In order to find dry points to establish the theoretical dry line, we must first understand the distribution of points in the space feature. In the VFC_LST feature space, some noise points distributed below the theoretical wet line in the bottom of the feature space (Figure 2) actually represent cloud-contaminated pixels that have a lower temperature than that of the land surface. The higher location of the point means that the soil corresponding to the point is dryer than the data suggests. So, in the VFC_LST feature space, three or more points satisfying the following requirements are chosen as dry points: a) the points are on a line and the line cannot pass through the scatter. If the line passes through the scatter, the line is not the theoretical dry line. b) land surface temperatures are the highest among points with the same VFC value, so the two points (point1, point2) that have the highest land surface temperatures are selected. And c) only if we cannot find three or more endpoints meeting the requirements are two points meeting the requirements used. Keep in mind, though, that more points on the theoretical dry line will give a more accurate estimate of the STI values. A schematics figure of choosing two points can be seen in Figure 2.

Figure 2. Schematic figure of choosing the two dry points



By solving Eq. (17) and Eq. (18), the land surface temperatures of the two endpoints on the dry line, T_{s2} and T_{v2} , can be obtained.

$$T_1 = T_{v2} * f_1 + T_{s2} * (1 - f_1) \quad (17)$$

$$T_2 = T_{v2} * f_2 + T_{s2} * (1 - f_2) \quad (18)$$

where f_1 and f_2 are VFC values of the two points. T_{s2} and T_{v2} have the same meanings as those symbols in Eq. (11) and Eq. (14). T_1 and T_2 are the mixture land surface temperatures of Point1 and Point2, which are from the MOD11A1 data. STI for soil and vegetation can then be calculated by Eq. (11) and Eq. (14). Because Eq. (11) and Eq. (14) lack sky temperature, the net radiation of bare land and vegetation-covered areas are calculated by Eq. (19) and Eq. (20), respectively.

$$R_{ns} = S_0(1 - \alpha_s) + DLR - \varepsilon\sigma T_s^4 \quad (19)$$

$$R_{nv} = S_0(1 - a_v) + DLR - \varepsilon\sigma T_v^4 \quad (20)$$

where the S_0 is the downward shortwave radiance from the sun and sky, the DLR is the down longwave radiance from the sky, ε is emissivity of land, and σ is the Stefan-Boltzmann constant. In this experiment, the DLR was observed by Yucheng Station. The albedo values of bare land and full cover vegetation areas can be decomposed by Eq. (21) and Eq. (22) as proposed by Zhang in 2005 [12].

$$a_1 = a_v * f_1 + a_s * (1 - f_1) \quad (21)$$

$$a_2 = a_v * f_2 + a_s * (1 - f_2) \quad (22)$$

where a_1 and a_2 are mixture albedo values of point1 and point2 (from the MOD09GA data), and f_1 and f_2 are VFC values of point1 and point2.

In Eq. (11) and Eq. (14), t_1 is the time when the net radiance was equal to zero, and t_2 was the satellite overpass time. T_{s1} and T_{v1} were observed from Yucheng station. STI results of the seven days are listed in Table 1.

Table 1. STI results of seven days

Date	Julian Day	S_0	DLR	t_1	t_2	T_{s1}, T_{v1} (K)	$T_1(K)$	a_1	f_1	$T_2(K)$	a_2	f_2	STI for Vegetation	STI for Soil
March 10	69	680.9	245.3	8	11.1	273.44	301.7	0.215	0.071	298.4	0.2	0.322	0.031	0.015
March 17	76	737.3	258	7.5	11.2	275.01	301.34	0.2	0.087	297	0.193	0.6	0.04	0.022
March 30	89	720.8	276.9	7.5	10.7	279.15	306	0.2	0.083	301.8	0.23	0.564	0.026	0.018
April 4	94	774.4	261.1	7	11	275.82	306.9	0.256	0.085	303.3	0.231	0.44	0.03	0.015
April 11	101	799.8	281.5	7	11	278.06	310.8	0.245	0.07	302.9	0.222	0.65	0.034	0.015
April 18	108	880	268.9	7	11.2	281.29	307.44	0.179	0.089	301.3	0.244	0.639	0.043	0.027
April 24	114	882	278.9	6	10.6	278.71	307.8	0.295	0.1	304.6	0.246	0.576	0.035	0.02

S_0 is the downward shortwave radiance from the sun (in W/m^2) and the sky. DLR is the down longwave radiance from the sky (in W/m^2), t_1 is the start time and t_2 is the end time in local hours, and T_{s1} and T_{v1} are the land surface temperatures at time t_1 for bare soil area and vegetation covered area, respectively. T_1 and T_2 are land surface temperature values of the two endpoints, a_1 and a_2 are albedo values of the two endpoints, and f_1 and f_2 are VFC values of the two endpoints. The STI for Soil and the STI for Vegetation are simplified thermal inertia values for Soil and Vegetation (in $cal \cdot cm^{-2} \cdot s^{-1/2} \cdot ^\circ C^{-1}$), respectively.

3.1.3. Selecting the most suitable STI result

The results in Table 1 show that among the seven days, 0.026 is the smallest STI for vegetation and 0.015 is the smallest STI for soil. Therefore, $P_{sd} = 0.015$ and $P_{vd} = 0.026$ (both in $\text{cal} \cdot \text{cm}^{-2} \cdot \text{s}^{-1/2} \cdot \text{°C}^{-1}$).

3.2 Laboratory experiment to measure the STI

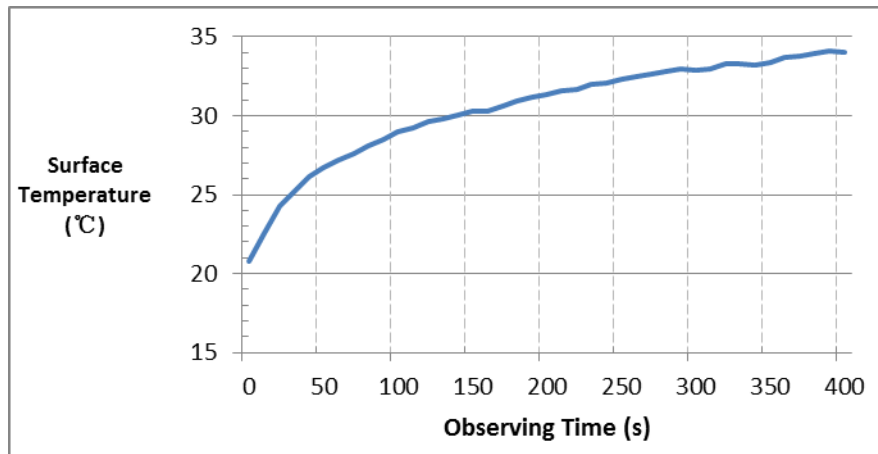
Thermal inertia is an inherent characteristic of soil, and it does not change with the measurements or the meteorological condition. Therefore, in order to assess the accuracy of the simplified thermal inertia values, three samples—including dry clay soil, dry sand soil, and full cover vegetation—are used in this experiment. In order to prepare the full cover vegetation sample, fresh tree leaves were inserted into a bucket filled with dry sand soil. The VFC value of the full cover vegetation sample is regarded as 1 because of the full cover, and the transpiration is 0. The equipment used in this experiment is shown in the Table 2.

Table 2. Equipment used in the laboratory experiment

Equipment	Specification of the accuracy and Unit	Functionality
Net pyranometer	$\pm 2\%$, w/m^2	Measuring net radiance
Lamp	Constant radiance at 275w/m^2	Providing downward shortwave and longwave radiation
Infrared thermometer	Model name: Raytek MX4, $\pm 1\text{°C}$, automatic recording	Measuring surface temperature

Before the lamp used to simulate the solar radiation was turned on in this experiment, samples had been placed in the laboratory for approximately 24 hours in order for the samples to reach the same temperature as that of the laboratory environment. During the experiment (once the lamp was turned on), the net radiation and the surface temperature were automatically recorded at an interval of 10 seconds. For the dry clay soil, the curve of surface temperature change over time is shown in Figure 3. It can be seen from Figure 3 that the rate of temperature rising becomes smaller as time goes by. This is because it takes a few minutes for the sample's temperature and the surrounding air temperature to approach equilibrium. In order to achieve a better accuracy in the calculations, only the first 10 measurements are used to compute the STI.

Figure 3. The change of surface temperature over time for dry clay soil



The results of STI measurement are shown in Table 3. It can be seen from Table 3 that STI values from the laboratory measurements are very close to the results estimated in 3.1. The STI values for dry soil and vegetation both have a bias below 0.005. The laboratory experiment verifies that the STI estimates from 3.1 are reasonable.

Table 3. Results of STI

Samples	laboratorial measured values	Estimated results
	($\text{cal} \cdot \text{cm}^{-2} \cdot \text{s}^{-1/2} \cdot \text{°C}^{-1}$)	($\text{cal} \cdot \text{cm}^{-2} \cdot \text{s}^{-1/2} \cdot \text{°C}^{-1}$)
Dry clay soil	0.0122	0.015
Dry sandy soil	0.0144	
Full covered vegetation	0.0223	0.026

4. Regional application of DDTI and the ET estimation

4.1 Study area

The central south region of the North China Plain, which has a boundary of latitude between 35°N and 37.5°N and longitude between 115°E and 117.5°E, is chosen as the study area. The study area belongs to the zone of the continental monsoon climate, which has four clearly distinct seasons. In the spring, it is dry and sees little rain, while in summer, it is very warm and rainy. The annual precipitation is in a range from 500mm to 700mm and changes greatly from year to year. The Yucheng experiment station is located in this region.

4.2 Computation processes of the two methods

Because the observation of ET at Yucheng station is not available after year 2011 and the year 2009 showed a high precipitation (101.6mm) in April and May, year 2009 was chosen to estimate the regional ET using DDTI. March 1 to May 31, 2009, was selected as the study period. Six clear days with cloud cover of less than 10% were chosen based on the MOD11A1 data. For the DDTI method, the most suitable simplified thermal inertia values described in 3.1 are applied to the six clear days of 2009 in order to determine the theoretical dry lines first. The simplified thermal inertia of dry soil P_{sd} , mean net radiation $\overline{R_{nsh}}$, start time t_{1h} , end time t_{2h} , and start temperature T_{1h} are fed into Eq. (13); then, the theoretical bare soil temperature T_{s2h} can be calculated. Similarly, T_{v2h} can be obtained by Eq. (16). After identifying the two endpoints on the theoretical dry line, the theoretical dry line can be determined. For the heat energy balance method, two endpoints are obtained by Eq. (5) and Eq. (6). The daily maximum air temperatures as observed separately by eleven weather stations in the study area were used as the daily air temperatures in the computations.

During the period of study, MOD11A1 data, from the land surface temperature product from Moderate-resolution Imaging Spectroradiometer (MODIS), were processed by the MODIS Reprojection Tool (MRT). Other data variables, such as albedo, LAI, NDVI, and VFC, were processed by the following approaches, with the MOD09GA products being used as the original input.

1) Albedo

$$\alpha = 0.039\alpha_1 + 0.504\alpha_2 - 0.071\alpha_3 + 0.105\alpha_4 + 0.252\alpha_5 + 0.069\alpha_6 + 0.101\alpha_7 \quad (23)$$

where $\alpha_1 \sim \alpha_7$ are the 11th ~ 17th bands in the MOD09GA product [22].

2) NDVI

$$NDVI = \frac{\alpha_1 - \alpha_2}{\alpha_1 + \alpha_2} \quad (24)$$

where α_1 and α_2 are the 13th and 14th band in the MOD09GA product.

3) VFC

$$VFC = \frac{NDVI - NDVI_{min}}{NDVI_{max} - NDVI_{min}} \quad (25)$$

where $NDVI_{max}$ is the maximum value in the NDVI data and $NDVI_{min}$ is the minimum value in the NDVI data.

In this paper, the slope of the theoretical wet line is set to zero. It implies that bare soil or a full cover vegetation area where there is no water stress has the same surface temperature as the theoretical wet line. The temperature of regional bodies of water within the study area is selected as the intercept of the theoretical wet line instead of the minimum LST value since the minimum LST value can correspond to a contaminated pixel due to cloud cover.

During the experiment, the Bowen ratio of soil and the Bowen ratio of vegetation can be calculated by the layered energy-separating algorithm of Bowen Ratio. Formulas are provided in Eq. (26, 27) [12,18]. Then, the available energy can be separated into soil evaporation and vegetation transpiration. A detailed introduction can be found in the literature [12,18].

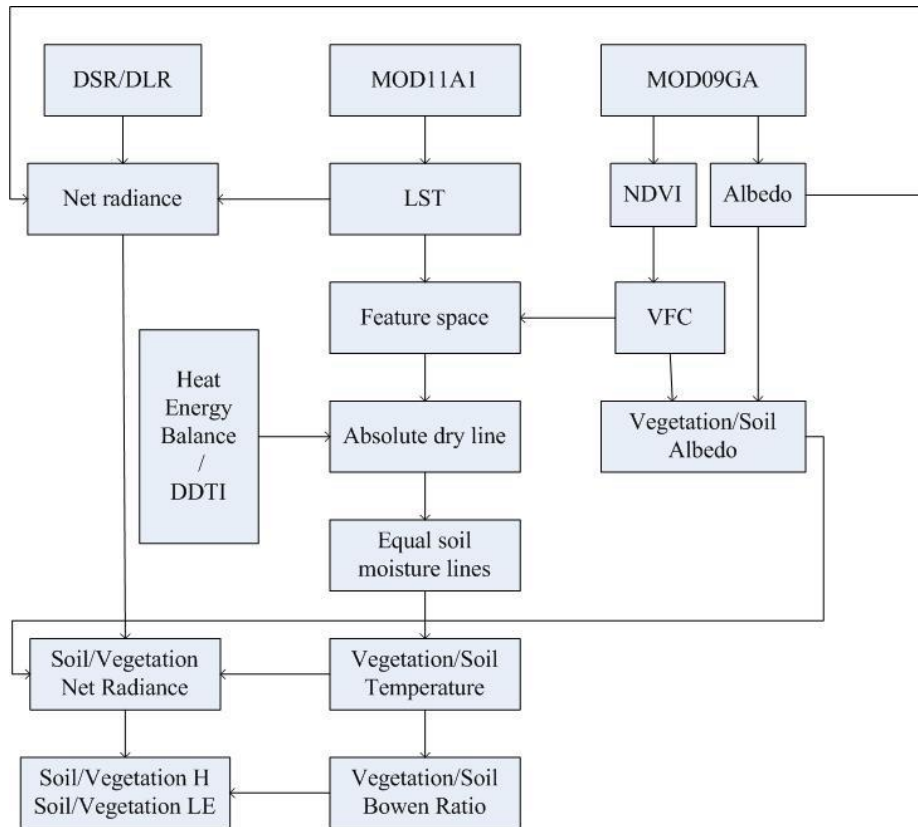
$$\beta_{si} = \frac{T_{sl} - T_{ss}}{T_{sl} - T_{si}} - 1 \quad (26)$$

$$\beta_{vi} = \frac{T_{vl} - T_{vs}}{T_{vl} - T_{vi}} - 1 \quad (27)$$

where T_{sl} is the maximum value of separated soil temperature, T_{ss} is the minimum value of separated soil temperature, T_{vl} is the maximum value of separated vegetation temperature, T_{vs} is the minimum value of separated vegetation temperature, T_{si} is the separated soil temperature of pixel i , and T_{vi} is the separated vegetation temperature of pixel i .

A flow chart showing the whole process is provided in Figure 4. The main difference between the two methods is how the theoretical dry line is determined.

Figure 4. Flow chart of the ET estimation process



4.3 Results

Two methods were adopted to evaluate the results: the first by comparing the locations of theoretical dry lines and the second by comparing the Evaporative Fractions from the two methods (DDTI and the heat energy balance method).

4.3.1 The location of theoretical dry line

The measured locations of theoretical dry lines resulting from the two methods are shown in Figure 5. Using historical precipitation data from the China Meteorological Sharing Service System, we have compared data from March 18, April 9, April 21, April 25, April 26, and May 23 with that of the ten days immediately prior to these dates in order to comparatively describe the selected dates as either dry periods or wet periods. The cumulative precipitation from March 18 and April 9 was approximately 2mm and 1mm, respectively. These two days are considered to be dry periods. The data from April 21, April 25, April 26, and May 23 show a large cumulative precipitation (approximately 30mm), so these four days are considered to be wet periods. It can be seen from Figure 5 that the locations of theoretical dry lines determined by the heat energy balance method are close to or pass through the scatter cloud, so the lines are not the theoretical dry lines in wet conditions. However, locations of theoretical dry lines determined by DDTI method are all above the scatter cloud, indicating that the line from DDTI shows a dryer condition than that from the heat energy balance method. The DDTI method presented in this paper can be used not only in two-layer remote sensing models, but also in one-layer schemes.

The evapotranspiration results on March 18 and April 21 of 2009 by the DDTI method are shown in Figure 6. These two days are representative of dry days and wet days. It can be seen from Figure 6 that the evapotranspiration on April 21 is larger than that of March 18. In both images, the areas with the largest evapotranspiration are bodies of water. Since the northwest region of the study area was mainly composed of cotton growing area, it was bare land in March and April, so evapotranspiration is much less than in other areas, which are winter wheat fields or mountain forest. Areas with no evapotranspiration values (shown in white) are cloud-contaminated pixels.

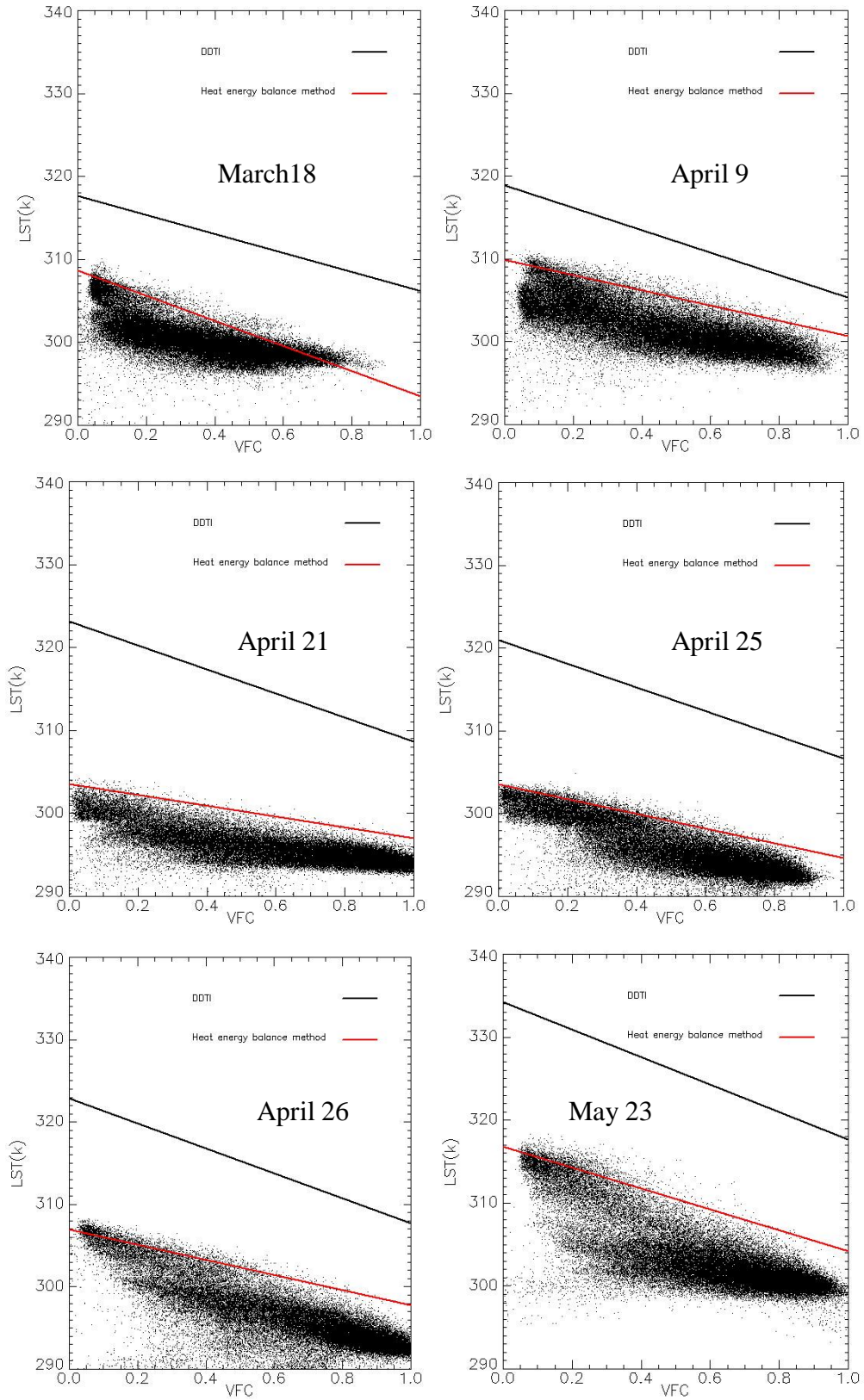
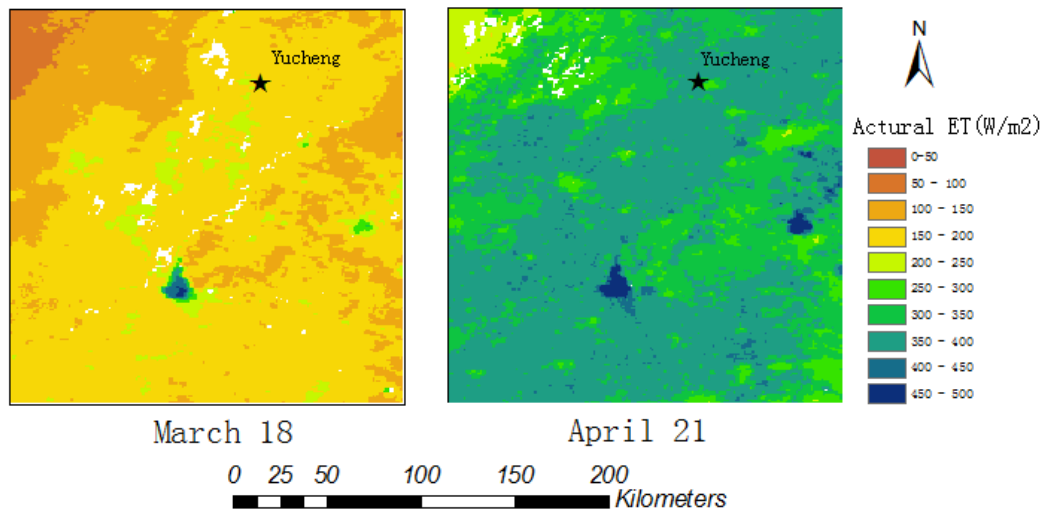
Figure 5. Locations of the theoretical dry lines from two methods.

Figure 6. Regional ET of March 18 and April 21.



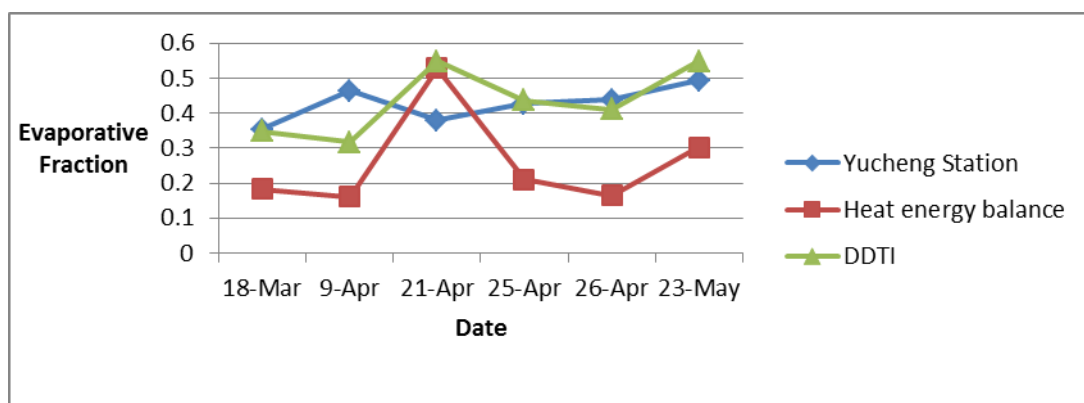
4.3.2 Comparison of Evaporative Fraction from the two methods

In order to further analyze the quality of the theoretical dry line by DDTI, the Evaporative Fraction (EF) was selected as a criterion to evaluate the two methods. EF is defined as the ratio of ET to the available energy [23].

$$EF = \frac{LE}{R_n - G} \tag{28}$$

EF values observed by Yucheng station, estimated by the heat energy balance method and by DDTI in the six clear days, are shown in Figure 7. When compared with the in situ measurements of EF at Yucheng Experimental Station, the ET model based on DDTI reproduces the pixel scale EF with an RMSE of 0.095, which is much lower than that based on the heat energy balance method (an RMSE of 0.224). Also, the bias between DDTI and in situ measurements is 0.069, lower than the bias of the heat energy balance method, which is 0.168. It shows that the DDTI method provided more accurate estimates than did the heat energy balance method.

Figure 7. Comparison of EF of the two methods



5. Conclusions

In this study, we developed a new method named DDTI to determine the theoretical dry line. The Simplified Thermal Inertia was first estimated by satellite observations in the North China Plain, and then validated by a laboratory experiment. DDTI was applied to the 6 clear days from 2009 in the North China Plain to estimate the regional ET. Finally, the EF observed by an experimental station was used to assess the accuracy of evaporation retrieval. Several conclusions can be obtained from this study:

- a) The STI values estimated in the North China Plain in dry situations are consistent with the measurements in the laboratory experiment, forming a solid basis for the DDTI method.
- b) The theoretical dry line determined by the DDTI is above all the scatter cloud in the feature space and appears more reasonable and robust than the line determined by the heat energy balance method.
- c) When compared with the in situ measurements of EF at Yucheng Experimental Station, DDTI reproduces the pixel scale EF with an RMSE (Root Mean Square Error) of 0.095, much lower than that based on the heat energy balance method (an RMSE of 0.224). Also, the bias between DDTI and the in situ measurements is 0.069, lower than the bias of the heat energy balance method, which is 0.168. This indicates that the DDTI method better estimates ET than does the heat energy balance method, and it can be applied to both wet conditions and dry conditions.

Acknowledgments

The work described in this publication has been supported by the National Basic Research Program of China 2013CB33406 and the National Natural Science Foundation of China (41271380, 41171286). Daily maximum air temperatures and precipitation data were provided by the China Meteorological Sharing Service System.

Author Contributions

Sujuan Mi wrote the manuscript with the contributions from all co-authors and was responsible for the research design, data preparation, and analysis. Hongbo Su, Renhua Zhang, and Jing Tian conceived and designed the research.

Conflicts of Interest

The authors declare no conflict of interest.

References and Notes

1. Choudhury, B.J. Estimating evaporation and carbon assimilation using infrared temperature

data: vistas and modeling , *Theory and Application of Optical Remote Sensing*, GhassemAsrar, John Wiley & Sons, New York ,1989, 628-690.

2. Kustas, W.P.; Norman, J.M. Use of remote sensing for evapotranspiration monitoring over land surfaces. *Hydrological Sciences Journal***1996**, 41, 495-517.
3. Moran, C.A.; Jackson, R.D. Assessing the spatial distribution of evapotranspiration using remotely sensed inputs. *Journal of Environment***1991**, 20: 725-737.
4. Jiang, L.; Islam, S. A methodology for estimation of surface evapotranspiration over large areas using remote sensing observations. *Geophysical research letters* **1999**, 26, 2773-2776.
5. Jiang, L.; Islam, S. Estimation of surface evaporation map over southern Great Plains using remote sensing data. *Water Resources Research***2001**, 37, 329-340.
6. Allen, R.G.; Tasymi, M.; Trezza, R. Satellite-based energy balance for mapping evapotranspiration with internalized calibration (METRIC) -model. *Journal of Irrigation and Drainage Engineering-ASCE***2007**, 133, 380-394.
7. Bastiaanssen, W.G.M.; Menenti, M.; Feddes, R.A.; Holslag, A.A.M. A remote sensing surface energy balance algorithm for land (SEBAL). *Journal of Hydrology***1998**, 198-213.
8. Su, Z.B. The Surface Energy Balance System (SEBS) for estimation of turbulent heat fluxes. *Hydrology and Earth System Sciences***2002**, 6, 85-99.
9. Roerink, G.J.; Su, Z.B.; Menenti, M. S-SEBI:A simple remote sensing algorithm to estimate the surface energy balance. *physics and chemistry of the earth(B)***2000**, 25, 147-157.
10. Norman, J.M.; Kustas, W.P.; Humes, K.S. Source approach for estimating soil and vegetation energy fluxes in observations of directional radiometric surface temperature. *Agriculture Forest Meteorology***1995**, 77, 263-293.
11. Kustas, W.P.; Norman, J.M. A Two-Source Energy Balance Approach Using Directional Radiometric Temperature Observations for Space Canopy Covered Surfaces. *Agronomy Journal***2000**, 92: 847-854.
12. Zhang, R.H.; Sun, X.M.; Wang, W.M.; Xu, J.P.; Zhu, Z.L; Tian, J. An operational two-layer remote sensing model to estimate surface flux in regional scale: Physical background. *Science in China Series D Earth Sciences***2005**. 48 Supp: 225-244.
13. Kustas, W.P.; Norman, J. M. Evaluation of soil and vegetation heat flux predictions using a simple two-source model with radiometric temperatures for partial canopy cover. *Agriculture Forest Meteorology***1999**, 94, 13-29.
14. Komatsu, T.S. Toward a Robust Phenomenological Expression of Evaporation Efficiency for Unsaturated Soil Surfaces. *Journal of Applied Meteorology***2003**, 42, 1330-1334.
15. Price, J.C. Using spatial context in satellite data to infer regional scale evapotranspiration.

*IEEE Transaction on Geoscience and Remote Sensing***1990**, 28: 940-949.

16. Moran, M.S.; Clarke, T.R.; Inoue, Y.; Vidal, A. Estimation crop water deficit using the relation between surface-air temperature and spectral vegetation index. *Remote Sensing Environment* **1994**, 49, 246-263.

17. Nishida, K.; Nemani, R.R.; Running, S.W; Glassy, J.M. An operational remote sensing algorithm of land surface evaporation. *Journal of Geophysical Research***2003**, 108 (D9), 4270.

18. Zhang, R.H; Tian, J.; Sun, X.M.; Chen, S.H.; Xia, J. Two improvements of an operational two-layer model for terrestrial heat flux retrieval, *Sensors***2008**, 8, 6165-6187.

19. Robin, L.F.; Philip, R.C.; Hugh, H.K. High-resolution thermal inertia derived from the thermal emission imaging system (THEMIS): thermal model and applications. *Journal of Geophysical Research***2006**, 111.

20. Zhang, R.H. Quantitative Model of thermal infrared remote sensing and ground experiments. Beijing: SciencePress, 2009; pp: 274-279.(In Chinese)

21. Price, J.C. On the Analysis of Thermal Infrared Imagery: The Limited Utility of Apparent Thermal Inertia. *Remote Sensing of Environment* **1985**, 18, 59-73

22. Liang, S.L. Narrowband to broadband conversions of land surface albedo 1 Algorithms. *Remote sensing of Environment***2000**, 76, 213-238.

23. Shuttleworth, W.J.; Gurney, R.J.; Hsu, A.Y.; Ormsby, J.P. FIFE: The variation in energy partition at surface flux sites. In A. Rango (Ed.), *Remote sensing and large-scale processes* (Proceedings of the IAHS third international Assembly, Baltimore, MD, May, 1989). IAHS Publication, 186, 67–74.